(4) Hayashi, H.; Hamada, F.; Nakajima, A. *Makromol. Chem.* **1977**, *178*, 827 and literature cited therein.
(5) Wolf, B. A. *J. Polym. Sci., Part A-2* **1972**, *10*, 847.
(6) Schulz, G. V.; Baumann, H.; Darskus, R. *J. Phys. Chem.* **1966**, *70*, 3647.
(7) Stickler, M. Ph.D. Dissertation, Mainz, 1977.
(8) Chu, S. G.; Munk, P. *J. Polym. Sci., Polym. Phys. Ed.* **1977**, *15*, 1163.
(9) Krigbaum, W. R.; Flory, P. J. *J. Am. Chem. Soc.* **1953**, *75*, 1775.
(10) Rahlwes, D.; Kirste, R. G. *Makromol. Chem.* **1977**, *178*, 1793.
(11) Fukuda, M.; Fukutomi, M.; Kato, Y.; Hashimoto, T. *J. Polym. Sci., Polym. Phys. Ed.* **1974**, *12*, 871.
(12) Tanaka, G.; Iami, S.; Yamakawa, H. *J. Chem. Phys.* **1970**, *52*, 2639.
(13) Rossi, C.; Bianchi, U.; Pedemonte, E. *Makromol. Chem.* **1965**, *89*, 95.
(14) Brandrup, J.; Immergut, E. H., Eds. "Polymer Handbook"; Wiley: New York, 1975.
(15) Norisuye, T.; Kawahara, K.; Teramoto, A.; Fujita, H. *J. Chem. Phys.* **1968**, *49*, 4330.
(16) Krigbaum, W. R. *J. Am. Chem. Soc.* **1954**, *76*, 3758.
(17) Noguchi, Y.; Aoki, A.; Tanaka, G.; Yamakawa, H. *J. Chem. Phys.* **1970**, *52*, 2651.
(18) Chinai, S. N. *J. Polym. Sci.* **1957**, *25*, 413.
(19) Olaj, O. F., private communication.

Block Copolymers near the Microphase Separation Transition. 3. Small-Angle Neutron Scattering Study of the Homogeneous Melt State

Frank S. Bates* and Mark A. Hartney

AT&T Bell Laboratories, Murray Hill, New Jersey 07974. *Received March 11, 1985*

ABSTRACT: A model set of six homogeneous (disordered) 1,4-polybutadiene–1,2-polybutadiene diblock copolymers containing perdeuterated 1,4-polybutadiene blocks have been examined by small-angle neutron scattering (SANS). Each of the SANS spectra exhibits a peak in the scattering intensity $I(q^*)$ at wave vector q^*, which diverges upon approaching the microphase separation transition (MST). These findings are in close agreement with the MST theory of Leibler, which predicts that $I(q^*)$ should depend on the product of the degree of polymerization N and interaction parameter χ; this provides a new, sensitive method of determining χ for polymer pairs. The theory fails to account for "domain" scattering, which results in an unpredicted increase in the level of $q < q^*$ scattering as $\chi N \rightarrow (\chi N)_{MST}$ in samples containing 18–25% 1,4-polybutadiene. This investigation corroborates our previous findings concerning the rheological properties of block copolymers near the MST.

Introduction

The combined effects of advances in quantitative theory, experimental techniques, and elegant synthetic chemistry over the past decade have brought about a revolution in the study of polymer–polymer thermodynamics. This synergistic, cross-disciplinary growth has been particularly evident in the area of block copolymers. Nevertheless, the limited availability of appropriate polymer pairs has focused most structure–property investigations of block copolymers on a select class of materials consisting of polystyrene and polydiene diblock and triblock copolymers. The inherent incompatibility of polystyrene and polydienes, together with the intrinsic differences in segment electron densities and chemical reactivities toward heavy metal oxidizing agents, and the availability of deuterated monomers make such copolymers useful substrates for studying the microphase-separated state by X-ray and neutron scattering and electron microscopy.[1-6] Furthermore, the elevated glass-transition temperature of polystyrene (~100 °C) imparts commercially important physical properties to these materials and an obvious motivation for understanding the structure–property relationships that govern their behavior.[7,8] The above-stated attributes that make polystyrene–polydiene block copolymers attractive candidates for studying microphase (ordered) structure and properties are largely detrimental in their application to the investigation of the microphase separation transition (MST). Chemical dissimilarity, which renders X-ray contrast and differential oxidizability utilized in obtaining phase contrast for electron microscopy, also leads to a large Flory interaction parameter ($\chi \cong 10^{-1}$) and a correspondingly low critical degree of polymerization for microphase separation ($N_c \cong 10^2$). The elevated glass-transition temperature that provides desirable mechanical properties limits any investigation of melt transitions to temperatures greater than ~100 °C. This greatly reduces the range of available experimental space and can lead to spurious and complicating chemistry. Nevertheless, several investigators have identified rheological[9-11] and X-ray scattering[12] phenomena in styrene–butadiene and styrene–isoprene block copolymers at elevated temperatures, which have been attributed to the microphase separation transition (MST). Yet it is apparent that the theoretical treatment[13] concerning the MST has far outdistanced our ability to quantitatively study such phenomena with conventional polystyrene–polydiene systems. This has motivated us to develop a more suitable model set of diblock copolymers with which to examine the detailed theoretical predictions and physical properties associated with this class of polymers near the MST.

The first of this series of papers[14] described the preparation and physical characteristics of a model set of 1,4-polybutadiene–1,2-polybutadiene diblock copolymers near the MST. Owing to a coupling between the structural order parameter and molecular diffusion, the phase state of these materials can be determined from rheological properties, as detailed in a second publication.[15] In the present and third report of this series, we address in detail the issue of structure in the homogeneous (disordered) melt state as determined by small-angle neutron scattering (SANS); the initial findings of this investigation have been published separately.[16] These results in large part corroborate the theoretical findings of Leibler[13] concerning disordered diblock copolymers, although the predicted scattering correlation function cannot account for all the

0024-9297/85/2218-2478$01.50/0

Table I
Characterization of 1,4-Polybutadiene–1,2 Polybutadiene Diblock Copolymers[a]

sample	Φ^b	$N_N \times 10^{-2}$ [c]	N_W/N_N [d]	$\chi \times 10^2$ [e]
BB1	0.47	4.7	1.05	1.15
BB3	0.18	5.8	1.04	0.6
BB4	0.23	9.4	1.04	0.6
BB5	0.25	15.9	1.07	0.6
BB8	0.61	8.0	1.05	1.20
BB10	0.50	10.5[d]	1.05	0.87

[a] The 1,4-polybutadiene block is perdeuterated, while the 1,2-polybutadiene block is fully protonated. [b] $\Phi = N_{1,4}/(N_{1,4} + N_{1,2})$, as measured by FTIR. [c] Degree of polymerization, as measured by membrane osmometry. [d] Measured by HPSEC. [e] Determined by fitting the predicted peak intensity (eq 2, corrected for polydispersity) to the SANS results obtained at 23 °C.

experimentally observed structural features. As suggested by Leibler, block copolymers indeed provide a unique and sensitive tool for measuring χ in bulk polymers. These findings are shown to be consistent with the previously reported[15] rheological transition that was attributed to the MST.

Experimental Section

Synthesis and Characterization. 1,4-Polybutadiene–1,2-polybutadiene (perdeuterio–normal) diblock copolymers were prepared by anionic polymerization techniques from perdeuterated and normal (protonated) butadiene monomers as previously described.[14] The resulting polymers contain a fully deuterated 1,4-block (89% 1,4 cis and trans and 11% 1,2 addition) and a fully protonated 1,2-block (>98% 1,2 addition). Number-average degree of polymerization $N = N_{1,4} + N_{1,2}$ was measured for each sample, except BB10, by membrane osmometry. N for sample BB10 and polydispersity indexes N_W/N_N for all samples were determined by high-pressure size-exclusion chromatograph (HPSEC) at 25 °C employing tetrahydrofuran as the mobile phase. The HPSEC instrument was calibrated for sample BB10 by using three previously characterized samples of similar composition (BB1, BB2, and BB7, as reported in ref 14). This method yielded a number-average degree of polymerization for BB10 within 4% of that determined from the synthesis stoichiometry. Sample composition $\Phi = N_{1,4}/N$ was measured by FTIR spectroscopy as previously reported.[14] The results of molecular characterization are summarized in Table I.

Small-Angle Neutron Scattering. Specimens for small-angle neutron scattering (SANS) were prepared by squeezing each liquid sample at room temperature between two 3 × 2 cm pieces of $^1/_{16}$-in. quartz separated by a $^1/_{16}$-in. spacer. A scattering cell containing sample BB10 was also prepared by using an aluminum ($^1/_{32}$ in. 6061 grade) and quartz window containing a $^1/_{32}$-in. spacer and a copper–constantin thermocouple embedded in the polymer. This latter assembly was used for measuring the temperature dependence of the scattering intensity from this sample. In order to avoid formation of bubbles and oxidative degradation, these scattering cells were assembled under vacuum (<10^{-3} torr), followed by epoxying and storage in an inert-gas environment. Actual sample thickness was carefully monitored by measuring the thickness of the windows and the overall scattering-cell dimensions.

Neutron-scattering spectra were obtained on the 30-m SANS instrument at the National Center for Small-Angle Scattering Research (NCSASR) located at Oak Ridge National Laboratory. Neutrons of 4.75-Å wavelength were collimated by using a 1.7-cm diameter circular source aperture and a 0.85-cm diameter circular sample aperture separated by 7.6 m. Scattered neutrons were counted with a 64 × 64 cm position-sensitive area detector located at distances of 14.8, 10, 6.5, and 2 m from the sample. Two-dimensional scattering data were corrected for background intensity, sample cell scattering, and sample thickness and transmission. As expected, these liquid samples produced isotropic two-dimensional scattering patterns that were radially averaged to one-dimensional form and reduced to units of absolute differential scattering cross section per unit solid angle (cm^{-1}) by calibrating the instrument with an irradiated aluminum secondary standard (A1-4). The A1-4 standard has been calibrated at NCSASR[17] on the basis of the incoherent scattering from water and vanadium and the coherent scattering from a well-characterized partially labeled polystyrene standard. This calibration procedure provides a reported precision of ±5%. Sample temperature was controlled between −7 and 90 °C (±0.5 °C) by circulating a thermostated fluid through a brass assembly containing the specimen cell.

Further details concerning the 30-m SANS facility at NCSASR can be found in ref 18.

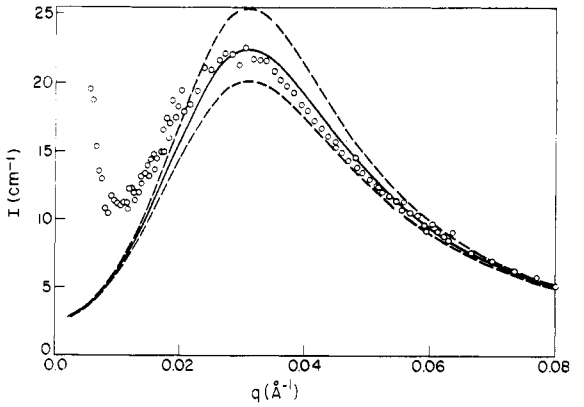

Figure 1. Coherent SANS results obtained from sample BB1 ($\Phi = 0.47$, $N_w = 4.9 \times 10^2$). Curves have been calculated by using eq 2 (corrected for polydispersity) based on $\chi = 1.15 \times 10^{-2}$ (solid curve), 1.25×10^{-2}, and 1.05×10^{-2} (upper and lower dashed curves, respectively).

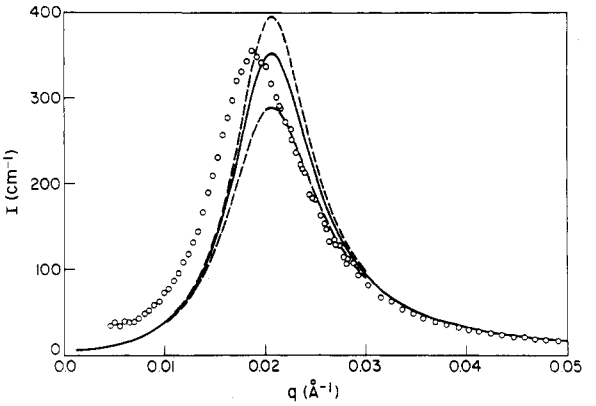

Figure 2. Coherent SANS results obtained from sample BB10 ($\Phi = 0.50$, $N_w = 11.0 \times 10^2$) at 23 °C. Curves have been calculated by using eq 2 (corrected for polydispersity) based on $\chi = 8.72 \times 10^{-3}$ (solid curve), 8.78×10^{-3}, and 8.60×10^{-3} (upper and lower dashed curves, respectively). As discussed in the text, the failure of the theory to predict the scattering peak location q^* results from the assumption of ideal (Gaussian) chain statistics.

Results

The measured scattering intensity represents the sum of incoherent and coherent scattering events.[19] Incoherent scattering cross sections for normal 1,2-polybutadiene and perdeuterio-1,4-polybutadiene were determined by measuring the angular independent intensity scattered by samples of each homopolymer (B1 and B2, as reported in ref 14). SANS spectra obtained from the six diblock copolymers have been corrected for incoherent scattering by subtracting a weighted sum of the corresponding homopolymer incoherent scattering intensities; the resulting coherent SANS spectra are given in Figures 1–6. Within experimental error, the data from samples BB1 and BB3 (Figures 1 and 4) are consistent with the previously reported experiments[16] that were conducted with these samples at the National Bureau of Standards. All six diblock copolymers examined exhibit a maxima in scattering intensity between $q = 0.01$ and 0.03 $Å^{-1}$ which de-

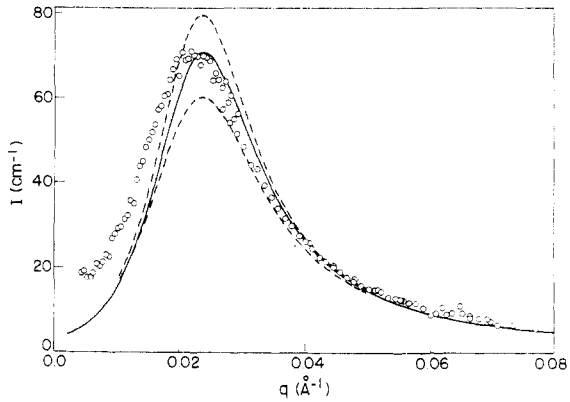

Figure 3. Coherent SANS results obtained from sample BB8 ($\Phi = 0.61, N_w = 8.4 \times 10^2$). Curves have been calculated by using eq 2 (corrected for polydispersity) based on $\chi = 1.20 \times 10^{-2}$ (solid curve), 1.23×10^{-2}, and 1.15×10^{-2} (upper and lower dashed curves, respectively).

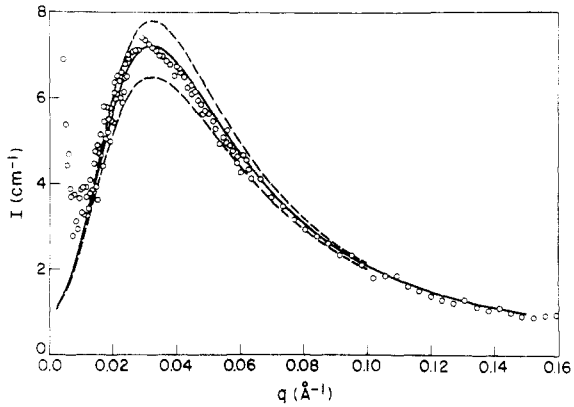

Figure 4. Coherent SANS results obtained from sample BB3 ($\Phi = 0.18, N_w = 6.0 \times 10^2$). Curves have been calculated by using eq 2 (corrected for polydispersity) based on $\chi = 6 \times 10^{-3}$ (solid curve), 8×10^{-3}, and 3×10^{-3} (upper and lower dashed curves, respectively).

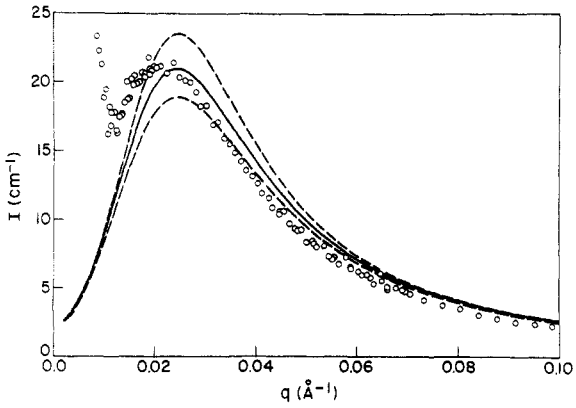

Figure 5. Coherent SANS results obtained from sample BB4 ($\Phi = 0.23, N_w = 9.8 \times 10^2$). Curves have been calculated by using eq 2 (corrected for polydispersity) based on $\chi = 6 \times 10^{-3}$ (solid curve), 7×10^{-3}, and 5×10^{-3} (upper and lower dashed curves, respectively).

rives from the correlation hole effect (see below). With the exception of the data from sample BB8, these results are replotted in Figures 7 and 8 in order to facilitate comparison of the scattering characteristics at relatively constant composition ($0.18 \leq \Phi \leq 0.25$ and $0.47 \leq \Phi \leq 0.50$, respectively) and varying degree of polymerization. Figure 7 also includes the purely incoherent scattering results obtained from sample B1, a fully protonated 1,2-polybutadiene homopolymer.[14]

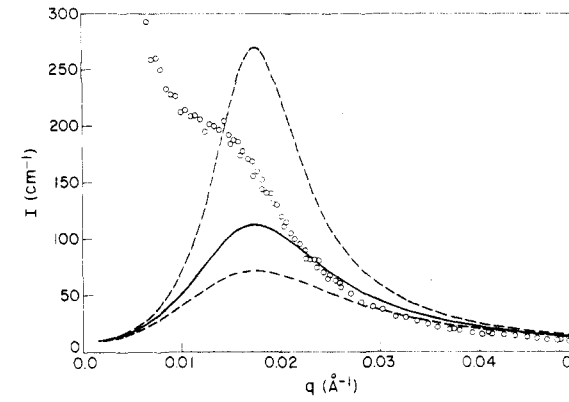

Figure 6. Coherent SANS results obtained from sample BB5 ($\Phi = 0.25, N_w = 17.0 \times 10^2$). Curves have been calculated by using eq 2 (corrected for polydispersity) based on $\chi = 6 \times 10^{-3}$ (solid curve), 7×10^{-3}, and 5×10^{-3} (upper and lower dashed curves, respectively). Deviation from the prediction at low q derives from domain-like scattering as discussed in the text.

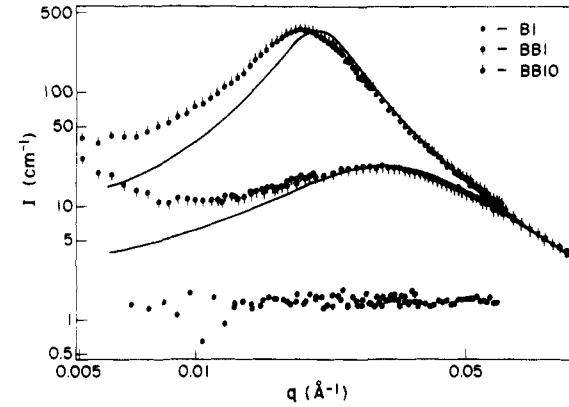

Figure 7. Effects of increasing χN near the critical composition at constant temperature, $T = 23$ °C. $\chi N_w = 5.7$ for sample BB1 ($\Phi = 0.47$) and 9.6 for sample BB10 ($\Phi = 0.50$); the spinodal point for $\Phi = 0.50$ is calculated to be $(\chi N)_s = 10.2$. (See Figure 13.) The curves correspond to the solid curves given in Figures 1 and 2. Sample B1 is a protonated 1,2 polybutadiene homopolymer that is characterized by purely incoherent scattering.

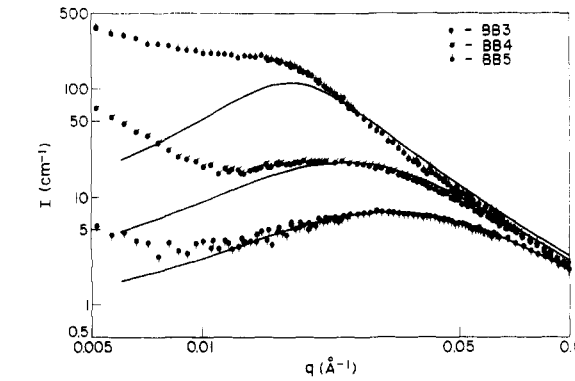

Figure 8. Effects of increasing χN at compositions $0.18 \leq \Phi \leq 0.25$. $\chi N_w = 3.6$, 5.9, and 10.2 for samples BB3, BB4, and BB5, respectively; the spinodal point for $\Phi = 0.25$ is calculated to be $(\chi N)_s = 13.5$. (See Figure 13.) The curves correspond to the solid curves given in Figures 4–6. Scattering at low q, in large excess of the theoretical prediction, derives from domain-like scattering as discussed in the text.

Sample BB10 was examined at 16 separate temperatures between −7 and 90 °C during two heating and cooling cycles. Spectra obtained at four representative temperatures are presented in Figure 9, and the measured peak intensities for all temperatures as listed in Table II. As described below, the sensitivity to changes in temperature

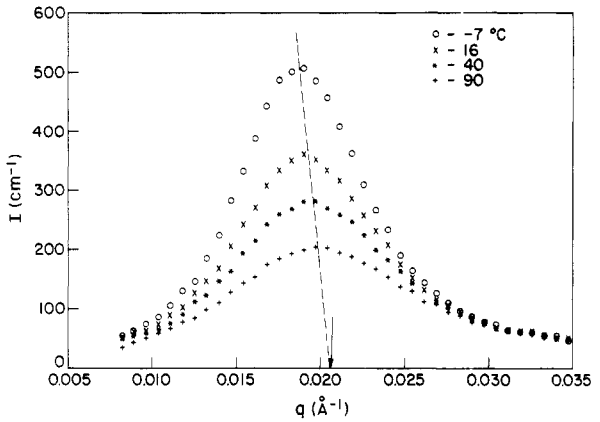

Figure 9. Representative SANS spectra of sample BB10 as a function of temperature. Because this sample lies near the spinodal point $(\chi N)_s = 10.2$ (Figure 13), small variations in χ, brought about by changes in temperature, produce large effects on the scattering peak intensity; for $T = 90$ °C, $\chi N_w = 9.15$, while at $T = -7$ °C, $\chi N_w = 9.78$. Increasing χN brings about an increasing deviation from ideal (Gaussian) chain statistics that is evidenced by the movement of the peak position q^*, as indicated by the dashed line. Theory (eq 2) predicts $q^* = 2.06 \times 10^{-2}$, as given by the arrow, independent of χN.

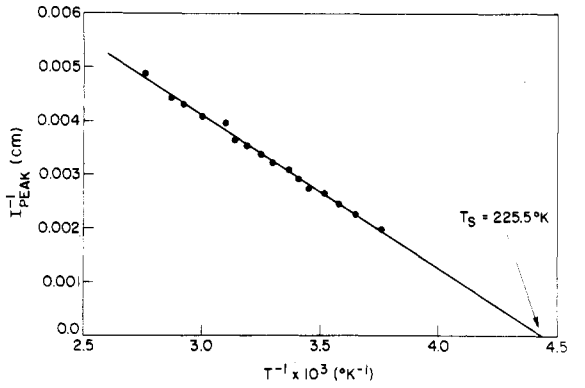

Figure 10. Determination of the spinodal temperature $T_s = 225.5$ K based on the peak intensities given in Table II and illustrated in Figure 9.

exhibited by this material results from the close proximity of this sample to the spinodal point in phase space. (See Figure 13.) Sample BB10 responded to temperature changes faster than the time required to record transient behavior. This is a natural consequence of the small distances over which composition fluctuations develop in disordered block copolymers, consistent with the previously reported rheological properties of diblock copolymers above the microphase separation transition temperature.[15] Reciprocal peak intensity ($0.018 \leq q^* \leq 0.020$) is plotted vs. inverse temperature for the results obtained at all 16 temperatures in Figure 14, yielding a spinodal temperature of 225.5 K. These results exhibit no sample history (heating vs. cooling) dependence, confirming that equilibrium had been established at each temperature.

Analysis

SANS Results. The coherent intensity scattered for unit volume of block copolymer $I(q)$ is related to the product of the sample scattering power (contrast factor) and structure factor $\tilde{S}(q)$

$$I(q) = VN_a[(b_{1,4}/V_{1,4}) - (b_{1,2}/V_{1,2})]^2\tilde{S}(q) \qquad (1)$$

where $V_{1,4}$ and $b_{1,4}$ are the molar volume and coherent scattering length for a 1,4-polybutadiene segment, N_a is Avogadro's number, and $V = \Phi V_{1,4} + (1 - \Phi)V_{1,2}$. Segment

Table II
Temperature Dependence of the Peak Scattering Intensity near the Spinodal Point (Sample BB10)

temp, K	$I(q^*)$, cm^{-1}	$\chi \times 10^3$ [a]
266	510	8.89
274	446	8.84
279	409	8.80
284	378	8.76
289.5	364	8.74
293	342	8.70
297	324	8.67
303	312	8.65
310	297	8.62
313	283	8.58
318	274	8.56
323	253	8.50
333	245	8.48
343	233	8.44
348	226	8.41
362.5	205	8.32

[a] Obtained by equating the predicted peak intensity (eq 2, corrected for polydispersity) to $I(q^*)$.

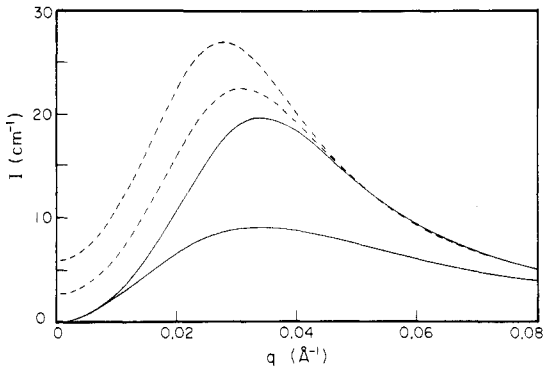

Figure 11. Effects of χN and polydispersity on the theoretical scattering function for homogeneous diblock copolymer (eq 2): $N_W/N_N = 1$, $\chi N = 0$ and 5.68, lower and upper solid curves, respectively; $\chi N = 5.68$, $N_W/N_N = 1.05$ and 1.1, lower and upper dashed curves, respectively.

molar volumes $V_{1,4} = 60.3$ and $V_{1,2} = 60.9$ cm^3/mol were determined at 23 °C by using a density gradient column technique. The coherent scattering lengths for perdeuterio and normal butadiene are given by the sum of the reported[19] atomic coherent scattering lengths, $b_{1,4} = 6.66 \times 10^{-12}$ and $b_{1,2} = 0.416 \times 10^{-12}$ cm.

According to Leibler[13] the structure factor for a homogeneous diblock copolymer melt is given by

$$\tilde{S}(q) = N[F(q) - 2\chi N]^{-1} \qquad (2)$$

where

$$F(q) = \frac{g_1(R)}{g_1(R_1)g_1(R_2) - \frac{1}{4}[g_1(R) - g_1(R_1) - g_1(R_2)]^2}$$

$$g_1(x) = 2[q^2x^2 + \exp(-q^2x^2) - 1]/R^4q^4$$

$$R^2 = R_1^2 + R_2^2$$

$g_1(x)$ is the correlation function for Gaussian chains[20] where R_1 and R_2 are the radii of gyration of each block

$$R_1^2 = a_{1,4}^2N_{1,4}/6 \qquad R_2^2 = a_{1,2}^2N_{1,2}/6 \qquad (3)$$

The segment (Kuhn) lengths $a_{1,4} = 6.7$ Å and $a_{1,2} = 5.9$ Å have been estimated from literature data as previously described.[16] Equation 2 is illustrated in Figure 11 for two values of χN ($\chi N = 0$ lower solid curve, $\chi N = 5.68$ upper solid curve) based on a composition and weight-average degree of polymerization N_W corresponding to sample BB1 (Table I).

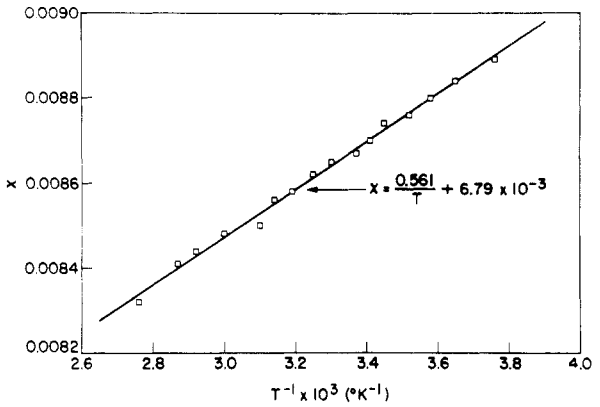

Figure 12. Temperature dependence of the interaction parameter χ based on the peak scattering intensities from sample BB10 and the prediction of eq 2 (corrected for polydispersity).

Leibler and Benoit[21] have predicted that polydispersity should strongly influence the low q scattering behavior of noninteracting ($\chi = 0$) block copolymers. We have adopted their approach in estimating the effects of a small amount of polydispersity on our calculated scattering intensity by substituting $\overline{Ng_1(x)}$ as given in the Appendix for $Ng_1(x)$, used in obtaining eq 2.[13] In doing so we make the following assumptions: (a) Polydispersity arises mainly through the polymerization kinetics that can be modeled with a Shultz–Zimm distribution.[21] (b) The overall diblock copolymer polydispersity $k = (N_W/N_N - 1)^{-1}$ can be related to each block polydispersity by[22] $k^{-1} = k^{-1}_{1,4}\Phi^2 + [k^{-1}_{1,2}(1 - \Phi)^2]$. Since $k_{1,4}/k_{1,2}$ cannot be independently determined by HPSEC, we further presume that $k_{1,4} = k_{1,2}$; calculations indicate that the predicted scattering profile is relatively insensitive to the ratio $k_{1,4}/k_{1,2}$ for the polydispersities listed in Table I. (c) The effects of polydispersity can be accounted for in $\tilde{S}(q)$ by modifying $F(q)$ on the basis of the prediction for ideal noninteracting chains. (See Appendix.)

The influence of this polydispersity correction on the predicted scattering intensity is demonstrated in Figure 11 for $\chi N = 5.68$ (dashed curves). Increasing N_W/N_N both increases the predicted intensity at low scattering wave vector and shifts the scattering peak to lower q. It should be noted the $N_W/N_N = 1.05$ corresponds to the HPSEC-determined polydispersity for sample BB1 (Table I). The effects of polydispersity also influence the phase diagram as discussed below.

On the basis of the characterization data listed in Table I we have fit the SANS results presented in Figures 1–6 with the polydispersity-corrected version of eq 2 by adjusting χ so as to bring the predicted peak intensity into agreement with the experiments (solid curves). These experimentally determined interaction parameters are also given in Table I. It should be stressed that there are no other adjustable parameters in this analysis. The sensitivity of the predicted peak intensity to χ is also indicated (dashed curves) in these figures and discussed in the following section. Best-fit predictions are reproduced in Figures 7 and 8 (solid curves).

We have also determined the temperature dependence of χ at $\Phi = 0.50$ from the temperature-dependent peak intensities obtained from sample BB10 (Table II). These results, which are listed in Table II and plotted in Figure 12, can be well represented by a linear function of temperature

$$\chi(\Phi = 0.50) = 0.561/T + (6.79 \times 10^{-3}) \qquad (4)$$

and are further discussed below. Equation 4 replaces our previous estimate[15] for $\chi(T)$.

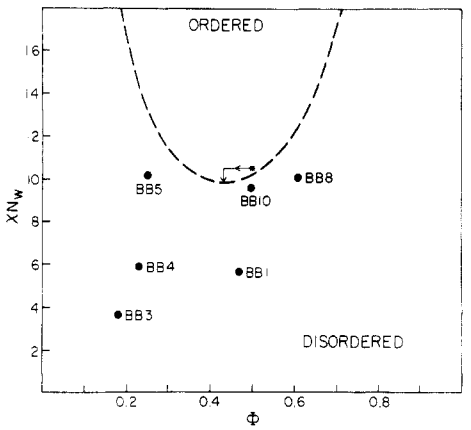

Figure 13. Calculated spinodal (stability) line for 1,4-polybutadiene–1,2-polybutadiene diblock copolymer based on a polydispersity index of $N_W/N_N = 1.05$. The asterisk represents the critical point calculated by Leibler:[13] $(\chi N)_c = 10.5$, $\Phi_c = 0.5$. Segment (Kuhn) length asymmetry shifts Φ_c to 0.43, while polydispersity shifts $(\chi N)_c$ to 9.87, as indicated by the arrows.

Phase Diagram. The correlation function for diblock copolymers (eq 2) exhibits a maximum at scattering wave vector q^*, which increases with increasing χN and diverges at the spinodal point, e.g., $S(q^*) \to \infty$ as $\chi N \to (\chi N)_s$. Taken over all Φ, these points define the spinodal curve, which represents the limit of stability for the disordered state. The minimum in the spinodal curve corresponds to the critical point; for symmetric ($a_1 = a_2$) monodisperse diblock copolymers the critical point occurs at $\Phi_c = 0.5$ and $(\chi N)_c = 10.5$. At all compositions except Φ_c, the spinodal point is preceded by the first-order microphase separation transition, $(\chi N)_{MST} < (\chi N)_s$.[13]

We have determined the spinodal curve for our model system by including the effects of polydispersity ($N_W/N_N = 1.05$) and unequal Kuhn lengths ($a_{1,4} = 6.7$ Å, $a_{1,2} = 5.9$ Å) in calculating $(\chi N)_s$ from eq 2. Increasing N_W/N_N serves to lower $(\chi N)_c$, while introducing asymmetry in the segment length shifts Φ_c; the combined result is that $\Phi_c = 0.43$ and $(N\chi)_c = 9.87$. The calculated phase diagram containing the experimentally determined sample locations (Table I) is presented in Figure 13. Although not calculated for this system, the MST is expected to be close to the spinodal curve by analogy with the symmetric case,[13,14] leaving all samples presently discussed within the homogeneous (disordered) region of phase space.

Discussion

Figures 1–8 provide a detailed picture of the structure of homogeneous diblock copolymer melts, in large part corroborating the theoretical findings of Leibler.[13] Nevertheless, the predictions systematically overestimate the location of the correlation hole (q^*) as $\chi N \to (\chi N)_s$ and fail to account for a significant level of scattering intensity at low scattering angles ($q < q^*$). These deviations can be understood in terms of the assumptions implicit in the theory as separately discussed below.

Correlation Hole Scattering ($q \sim q^*$). The peak observed in the SANS spectra derives from the correlation hole effect as originally described by de Gennes.[20,23] For $qR \gg 1$ segment density fluctuations resemble those in a simple binary blend, where the scattering intensity is given by

$$\tilde{S}(q) \cong \frac{2N\Phi(1 - \Phi)}{q^2R^2} \qquad (qR \gg 1) \qquad (5)$$

while over large distances ($qR \gg 1$), the assumption of bulk

incompressibility and the single-component nature of monodisperse block copolymer melts dictate that the scattering power fall to zero:

$$\tilde{S}(q) \cong 2N\Phi^2(1-\Phi)^2q^2R^2/3 \quad (qR \ll 1) \qquad (6)$$

This produces a peak in the homogeneous melt around $qR \sim 1$ *independent* of segment–segment interactions. Experiments with partially labeled polystyrene have confirmed this prediction of a correlation hole in the limit $\chi N \cong 0$.[24] Leibler[13] has extended this concept in calculating the structure factor for homogeneous block copolymer melts for which $\chi > 0$. This theory assumes Gaussian chain statistics, which specify that the composition fluctuations scale as $q^* \sim N^{1/2}$. Yet theory[25] and experiment[5,6] have demonstrated that in the ordered (microphase separated) state, $\chi N \gg (\chi N)_s$, microdomain structure scales as $q^* \sim N^{2/3}$. Therefore, we would expect the ideal chain statistics approximation to break down in the vicinity of $(\chi N)_s$.

The overestimation of q^* evidenced in all the predictions except that for sample BB3 is a direct manifestation of the deviation from Gaussian statistics. Far below the spinodal curve, the correlation hole (scattering peak) characterizing sample BB3 is quantitatively predicted in both shape and location (q^*) by eq 2 (Figure 4). Increasing χN by moving to either sample BB1 or BB4 shifts the experimentally observed q^* slightly below that of the prediction (Figures 1 and 5). This trend continues with further increases in χN, e.g., samples BB5 (Figure 6) and BB10 (Figure 2), although in the former case, the scattering at $q < q^*$ (see below) begins to obscure the correlation hole scattering. At room temperature, the calculated q^* for sample BB10 is 10% higher than that determined experimentally.

Because sample BB10 lies near the spinodal point (see Figure 13), varying temperature provides a direct measure of the transition away from Gaussian statistics, as indicated by the dashed line in Figure 9. Note that if this trend is extrapolated back to $\chi N = 0$, which corresponds to $I(q^*) = 40$, the predicted $q^* = 2.06 \times 10^{-2}$ Å^{-1} is essentially recovered, as indicated by the arrow. We have verified that these results do not derive from instrument resolution effects (finite pinhole size and detector resolution) using the method of Ramakrishnan;[26] e.g., smearing eq 2 with an instrumental smearing function produces some peak broadening but does not change q^*.

The predicted lattice spacing associated with yet larger values of χ, in the ordered region of phase space, for sample BB10 can be estimated by using the theory of Helfand.[25] Assuming a lamellar microstructure, we calculate that for $\chi N = 55$ and 110, $q^* = 0.0154$ and 0.0135 Å^{-1}, respectively, further confirming the nature of the trend observed in the disordered melt state.

Although Gaussian chain statistics begin to fail near the microphase separation transition, the mean-field assumption concerning the interactions can be independently shown to remain valid. Extrapolating the reciprocal peak intensity to 0 in Figure 10 establishes the stability temperature as $T_s = 225.5$ K. Near a stability limit the divergence in scattering intensity is related to the reduced value of χN by[20]

$$I(q^*) \sim [(\chi N)_s - (\chi N)]^{-\gamma} \qquad (7)$$

where γ is a universal exponent that is characterized by a mean-field value of unity.[27] Having demonstrated that $\chi \sim T^{-1}$, we can reduce eq 7 to

$$I(q^*) \sim [T^{-1}{}_s - T^{-1}]^{-\gamma} \text{ or } \left(1 - \frac{T_s}{T}\right)^{-\gamma} \qquad (8)$$

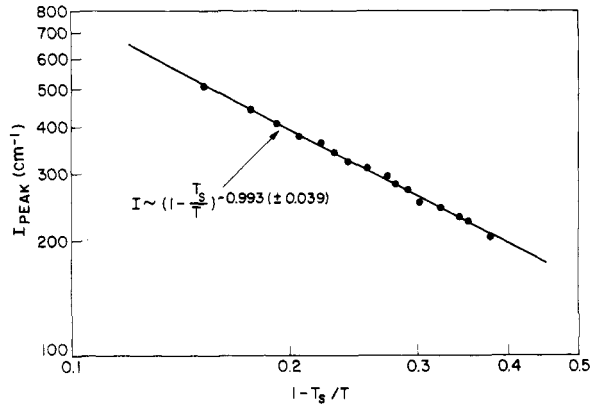

Figure 14. Reduced peak intensity plotted vs. reduced temperature, demonstrating the mean-field nature of the interactions driving ample BB10 to order as $\chi N \to (\chi N)_s$.

Peak intensity is plotted vs. reduced temperature in Figure 14 yielding $\gamma = 0.993 \pm 0.039$, confirming the mean-field character of the segment–segment interactions that drive this system to order.

Scattering at $q < q^*$. All six diblock copolymers examined scatter significantly more radiation at low wave vectors $q < q^*$ than is predicted by eq 2 (corrected for polydispersity). The combined efforts of careful synthetic procedures resulting in <5% w/w homopolymer contamination[14] and the use of liquid specimens prepared under vacuum conditions preclude the possibility that this scattering arises from artifacts such as homopolymer segregation[28] or the presence of voids. (Note the lack of any structural scattering from homopolymer sample B1 in Figure 7.) Instead, we believe that it is the failure of the theory to account for domain scattering which explains the discrepancy between the calculated and observed results for $q < q^*$. This conclusion can be best understood by examining the scattering behavior exhibited by microphase-separated block copolymers. In order to facilitate this discussion, the SANS results have been collected into two sets of nearly constant composition, as presented in Figures 7 and 8. Low q scattering from samples BB3, BB4, and BB5 ($\Phi = 0.18$, 0.23, and 0.25) and B1 and B10 ($\Phi = 0.46$ and 0.50) will be compared to the small-angle scattering obtained from spherical (and cylindrical) and lamellar block copolymer structures, respectively.

The intensity of radiation scattered at small angles by block copolymers containing spherical or cylindrical microstructure is proportional to the product of the single particle (domain) structure factor and an interparticle interference function.[1,6,29] What is termed the correlation hole (eq 2) in the disordered state corresponds to interparticle interference in the ordered state. On the basis of this analogy, the unpredicted intensity at $q < q^*$, which characterizes samples BB3, BB4, and BB5, is expected to derive from "domain-like" scattering. Scattering from spherical and cylindrical domains is proportional to the domain concentration c and volume V[1,6]

$$I_{\text{domain}}(q) \sim cV^2e^{-R_g^2q^2/3} \quad (R_gq < 1) \qquad (9)$$

where R_g is an effective particle radius of gyration. The form of the $q < q^*$ scattering for samples BB3, BB4, and BB5 is consistent with this (Guinier) expression. Assuming $R_g \sim N^{1/2}$ to $N^{2/3}$ (see above discussion on $q \sim q^*$ scattering), the intensity of the low-angle scattering from a collection of domains at constant domain volume fraction ($c \sim V^{-1}$) should scale as

$$I_{\text{sphere}}(0) \sim N^{3/2} \text{ to } N^2 \qquad I_{\text{cylinder}}(0) \sim N^1 \text{ to } N^{4/3} \qquad (10)$$

This is also consistent with our results; e.g., the contribution of the low q scattering to the observed SANS spectra increases dramatically with increasing N. (See Figures 4–6 and 8.) A quantitative description of this scattering behavior would require incorporating the changes in effective contrast accompanying an increase in χN, which is beyond the scope of this discussion. It should also be noted that these findings are not unique to this set of measurements. Roe et al.[12] have reported a SAXS spectra obtained from a disordered styrene–butadiene diblock copolymer ($\Phi = 0.25$) at high temperature that strongly resembles the SANS spectrum from sample BB5 (Figure 6).

Scattering from ordered lamellae is qualitatively different than that described above.[4,5] In this case, interparticle interference effects dominate and domain scattering is inversely related to the size of the ordered regions (grains). Therefore, increasing N in the disordered state in samples that are developing a lamellar morphology should in principle *decrease* the relative intensity of the $q < q^*$ scattering, since increasing χN increases the grain size. Indeed the SANS results from samples BB1 and BB10 (Figure 1, 2, and 7) confirm this expectation. In contradistinction to the previous situation, increasing N now diminishes the effects of $q < q^*$ scattering and brings the correlation hole prediction at low q into closer agreement with the experimental results (Figure 7).

These observations clearly indicate the origin of the disparity between the predicted and experimentally measured SANS results at low scattering wave vectors.

χ Parameter. The theory of Leibler[13] (eq 2) is based on the original lattice model description of χ,[30] which assumes that segment–segment interactions can be described entirely in terms of the energy of interaction between chemically different species:

$$\chi = [\epsilon_{AB} - \tfrac{1}{2}(\epsilon_{AA} + \epsilon_{BB})]/kT \qquad (11)$$

Neither the temperature (eq 4) nor composition (Table I) dependence exhibited by the experimentally determined interaction parameters support this assumption; others have made similar observations in studying binary polymer blends.[31–33] These results can be related to the inability of the classical theory to account for free volume and orientational entropy effects. More recently, modified lattice[34] and equation-of-state theories[35] have attempted to rectify these deficiencies implicit in the original lattice model treatment. For example, the large constant found in eq 4, representing 78% of χ at room temperature, suggests that the interaction parameter in large part reflects interaction (noncombinational) entropy rather than interaction energy.

In principle these considerations should be included in the derivation of the correlation function for homogeneous block copolymers, although in practice this would appear to be rather difficult. We can qualitatively assess these effects by examining the measured interaction parameter at different locations in phase space.

Far below the spinodal point the local composition deviates only slightly around the sample average, so that the measured χ should closely reflect the true interaction parameter for the overall sample composition. Hence, we have established the composition dependence of χ based on samples BB3, $\chi(\Phi = 0.18) = 0.6 \times 10^{-2}$, and BB1, $\chi(\Phi = 0.46) = 1.15 \times 10^{-2}$. Increasing χN at roughly constant sample composition does not seem to affect the measurement of χ, provided the sample remains well below the spinodal point, e.g., χ remains at approximately 0.6×10^{-2} for samples BB4 and BB5. In contrast, as $\chi N \rightarrow (\chi N)_s$, the local composition begins to fluctuate significantly about the sample average. Hence, the measured χ should reflect a value averaged over a range of compositions. Therefore, it is not surprising that the *effective* measured χ for sample BB10 lies between that determined for BB1 and BB3, $\chi(\text{BB10}) = 0.87 \times 10^{-2}$ at 23 °C. In other words, as the phase boundary is approached, the effective driving force for ordering is somewhat compensated by the development of composition fluctuations. As a result, the critical degree of polymerization calculated from the determination of χ at $\Phi \cong 0.5$, well below $(\chi N)_s$, underestimates the actual values by nearly 25%! In spite of these complications, the mean-field description of segment–segment interactions remains intact (Figure 14) and the correlation function accurately predicts the form of the scattering. (Note the above comments concerning the location of q^*.) It would be interesting to determine whether these same effects operate in binary blends of these polymers near critical points in phase space.

In a previous report[15] the interaction parameter was estimated at $T = 108$ °C for sample BB6 ($\Phi = 0.38$, $N_w = 1.4 \times 10^3$) on the basis of the rheological transition that accompanies the MST. According to Leibler[13] the MST at this composition occurs at $\chi N = 11.6$. (As discussed in the Analysis section, the true $(\chi N)_{MST}$ is probably approximately 10% lower owing to the effects of segment length asymmetry and polymer polydispersity.) The corresponding $\chi = 0.83 \times 10^{-2}$ is in close agreement with that determined from eq 4 at 108 °C, $\chi = 0.82 \times 10^{-2}$. That these values essentially agree *exactly* must be viewed as rather fortuitous, since these samples differ somewhat in composition and we have ignored the effects of isotopic labeling;[36] e.g., sample BB6 and BB10 contain normal and perdeuterio 1,4-polybutadiene, respectively. Nevertheless, these results evidence the success of Leibler's theory at predicting the behavior of block copolymers near the microphase separation transition and provide a motivation for future research concerning the phase behavior of this class of macromolecules.

Finally, an important point that warrants repeating is the nature of the thermodynamic phase boundary measured by SANS and mechanical spectroscopy (rheology). The divergence in $I(q^*)$, as determined by SANS, establishes the spinodal (stability) point denoted $(\chi N)_s$, while rheological measurements have been demonstrated[15] to provide the equilibrium (binodal) point, denoted $(\chi N)_{MST}$. The coupling between structural order and molecular diffusion in block copolymers renders both of these thermodynamic limits directly observable. In contrast, there is no equivalent method of establishing the equilibrium point in binary polymer blends.

Conclusions

This third in a series of articles devoted to studying block copolymers near the microphase separation transition has focused on examining the structural characteristics of a model set of homogeneous (disordered) 1,4-polybutadiene–1,2-polybutadiene diblock copolymers by small-angle neutron scattering (SANS). These results have been modeled by using the mean-field microphase separation transition (MST) theory of Leibler.[13] This theory quantitatively predicts the existence of a scattering peak in the homogeneous melt state, which depends solely on the product of the interaction parameter χ and the degree of polymerization N. The theory fails to account for a significant mount of low q scattering which is shown to derive from the domain-like structure that exists in the homogeneous state.

An important conclusion of this work is that these measurements provide a sensitive new method for deter-

mining χ as originally proposed by Leibler. Both the measured composition and temperature dependence of χ indicate that equation-of-state contributions to the mixing free energy strongly influence the phase behavior of these materials. Within experimental error, the effective χ parameter measured by SANS agrees with that determined from the previously reported rheological study.[15]

Acknowledgment. This research was made possible through the collective efforts of the staff of the National Center for Small-Angle Scattering Research (NCSASR), for which we are extremely grateful. Dr. George D. Wignall has been particularly helpful in this regard. It is also a pleasure to acknowledge Dr. Eugene Helfand for his helpful discussions.

Appendix

The correlation function for a diblock copolymer consisting of noninteracting ($\chi = 0$) blocks of N_1 and N_2 segments is given by[21]

$$\tilde{S} = (S_{11}S_{22} - S_{12}^2)/(S_{22} + 2S_{12} + S_{11}) \quad \text{(A-1)}$$

where

$$S_{11}(q) = Ng_1(R_1)$$

$$S_{22}(q) = Ng_1(R_2)$$

$$S_{12}(q) = S_{21}(q) = (N/2)[g_1(R) - g_1(R_2) - g_1(R_1)]$$

g_1 is a Debye function

$$g_1(R_1) = (2/q^4R^4)[q^2R_1^2 + \exp(-q^2R_1^2) - 1] \quad \text{(A-2)}$$

that assumes Gaussian chain statistics, $R_1^2 = a_1^2N_1/6$ and $R^2 = R_1^2 + R_2^2$ where a_1 represents the segment (Kuhn) length. Equation A-1 reduces to eq 2 (text) for $\chi = 0$. In order to estimate the effects of polydispersity on $\tilde{S}$, we adopt the approach of Leibler and Benoit[21] and calculate $\overline{Ng_1(x)}$ using a Shultz–Zimm distribution of block lengths:

$$\theta(n) = (k/n_N)^{k+1}n^k \exp[-(k/n_N)n/\Gamma(k+1)] \quad \text{(A-3)}$$

$\theta(n)$ is the probability that a block contains n segments where $k = (n_W/(n_N - 1))^{-1}$, and Γ denotes the Γ function. So as to simplify the following calculation, we neglect differences in segment lengths, $a_1 = a_2 = a$, whereby the Debye function can be expressed in terms of composition $\Phi = N_1/N$ and the degree of polymerization N. The average value $\overline{Ng_1(\Phi)}$ can now be determined as

$$\overline{Ng_1(\Phi)} = \int_0^\infty \int_0 \theta(N_1)\theta(N_2)\frac{2}{y^2} \times \left[\Phi y + \exp\left(-\frac{\Phi N y}{N}\right) - \frac{1}{N}\right] dN_2\, dN_1 \quad \text{(A-4)}$$

where $N = N_1 + N_2$ and $y = q^2a^2/6$. The general solution of eq A-4 for $\Phi \leq 0.5$ is

$$\overline{Ng_1(\Phi)} = \frac{2\bar{N}}{x^2}\left\{\frac{x}{2}\left(\frac{\Phi}{1-\Phi}\right)F(1,k+2;2k+3;z) + \frac{1}{(1-\Phi)(3-\lambda)}[(1 + \Phi x(\lambda - 1))^{-(k+1)}F(k+1,1;2k+2;z') - F(1,k+1;2k+2;z)]\right\} \quad \text{(A-5)}$$

and

$$\overline{Ng_1(1-\Phi)} = \frac{2\bar{N}}{x^2}\left\{\frac{x}{2}(F(1,k+1;2k+3;z) + \frac{1}{(1-\Phi)(3-\lambda)}[(1 + (1-\Phi)x(\lambda - 1)^{-k}F(1,k+1;2k+2;z'') - F(k+1,1;2k+2;z)]\right\} \quad \text{(A-6)}$$

where $x = q^2\bar{R}^2 = \bar{N}a^2/6$, $\lambda = N_W/N_N$ describes the polydispersity of each block, $F(a,b;c;z)$ denotes the hypergeometric function,[37] and

$$k = (2 - \lambda)/(\lambda - 1) \quad \text{(A-7)}$$

$$z = (1 - 2\Phi)/(1 - \Phi)$$

$$z' = 1 - \frac{\Phi}{1-\Phi}[1 + \Phi x(\lambda - 1)]^{-1}$$

$$z'' = 1 - \frac{\Phi}{1-\Phi}[1 + (1 - \Phi)x(\lambda - 1)]$$

The solution for $\overline{Ng_1(1)}$ is given by

$$\overline{Ng_1(1)} = \frac{2\bar{N}}{x^2}\left\{x + \frac{1}{(2-\lambda)}[(1 + x(\lambda - 1))^{-k} - 1]\right\} \quad \text{(A-8)}$$

Equations A-5 and A-6 reduce to the result presented by Leibler and Benoit[21] for the symmetric case $\Phi = 0.5$.

We account for the variation in segment lengths between 1,4-polybutadiene and 1,2-polybutadiene in calculating the polydispersity-corrected structure factor by noting the similarity between eq A-2 and eq A-5, A-6, and A-8. x in eq A-8 and outside the braces in eq A-5 and A-6 is computed by using $\bar{R}^2 = (a_{1,4}^2\bar{N}_{1,4} + a_{1,2}^2\bar{N}_{1,2})/6$. Within the braces in eq A-5 and A-6, x is calculated on the basis of the overall degree of polymerization $\bar{N}$, and the Kuhn length associated with the block being considered, e.g., $\bar{R}^2 = a_{1,4}^2\bar{N}/6$, is used to calculate x within the brackets for $\overline{Ng_1(\Phi)}$. The results reported in the text have been obtained by setting $\bar{N} = N_W$. In the limit $\lambda \to 1$, this polydispersity-corrected structure factor numerically reduces to that obtained from eq 2 (text).

Registry No. (Butadiene)·(butadiene-d_6) (copolymer), 98821-49-9; neutron, 12586-31-1.

References and Notes

(1) Bates, F. S.; Berney, C. V.; Cohen, R. E. *Macromolecules* **1983**, *16*, 1101.
(2) Bates, F. S.; Berney, C. V.; Cohen, R. E.; Wignall, G. D. *Polymer* **1983**, *24*, 519.
(3) Bates, F. S.; Cohen, R. E.; Berney, C. V. *Macromolecules* **1982**, *15*, 589.
(4) Hashimoto, T.; Nagatoshi, K.; Todo, A.; Hasegawa, H.; Kawai, H. *Macromolecules* **1974**, *7*, 364.
(5) Hashimoto, T.; Shibayama, M.; Kawai, H. *Macromolecules* **1980**, *13*, 1237.
(6) Hashimoto, T.; Fujimura, M.; Kawai, H. *Macromolecules* **1980**, *13*, 1660.
(7) Bates, F. S.; Cohen, R. E.; Argon, A. S. *Macromolecules* **1983**, *16*, 1101.
(8) Schwier, C. E.; Argon, A. S.; Cohen, R. E. *Polymer*, submitted.
(9) Chung, C. I.; Lin, M. I. *J. Polym. Sci., Polym. Phys. Ed.* **1978**, *16*, 545. Chung, C. I.; Gale, J. C. *J. Polym. Sci., Polym. Phys. Ed.* **1976**, *14*, 1149.
(10) Gouinlock, E.; Porter, R. *Polym. Eng. Sci.* **1977**, *17*, 534.
(11) Widmaier, J. M.; Meyer, G. C. *J. Polym. Sci., Polym. Phys. Ed.* **1980**, *18*, 2217.
(12) Roe, R.-J.; Fishkis, M.; Chang, J. C. *Macromolecules* **1981**, *14*, 1091.
(13) Leibler, L. *Macromolecules* **1980**, *13*, 1602.
(14) Bates, F. S.; Bair, M. E.; Hartney, M. A. *Macromolecules* **1984**, *17*, 1987.
(15) Bates, F. S. *Macromolecules* **1984**, *17*, 2607.
(16) Bates, F. S. *Macromolecules* **1985**, *18*, 525.
(17) Wignall, G. D., unpublished data.
(18) Koehler, W. C.; Hendricks, R. W.; Child, H. R.; King, S. P.; Lin, J. S., Wignall, G. D. In "Scattering Techniques Applied to Supramolecular and Nonequilibrium Systems"; Chen, S.-H.; Chu, B.; Nossal, R., Eds.; Plenum Press: New York, 1981; NATO Adv. Study Inst. Ser. No. B73.

(19) Bacon, G. E. "Neutron Diffraction", 3rd ed.; Oxford University Press: Oxford, 1975.
(20) de Gennes, P.-G "Scaling Concepts in Polymer Physics"; Cornell University Press: Ithaca, NY, 1979.
(21) Leibler, L.; Benoit, H. *Polymer* **1981**, *22*, 195.
(22) Ionescu, L.; Picot, C.; Dupplessix, R.; Duval, M.; Benoit, H.; Lingelser, J. P.; Gallot, Y. *J. Polym. Sci., Polym. Phys. Ed.* **1981**, *19*, 1033.
(23) de Gennes, P.-G. *J. Phys.* **1970**, *31*, 235.
(24) Boué, F.; Daoud, M.; Nierlich, M.; Williams, C.; Cotton, J. P.; Farnoux, B.; Jannik, G.; Benoit, H.; Dupplessix, R.; Picot, C. *Neutron Inelastic Scattering, Proc. Symp., 1977* **1978**, *1*, 563. Duplessix, R.; Cotton, J. P.; Benoit, H.; Picot, C. *Polymer* **1979**, *20*, 1181.
(25) Helfand, E.; Wasserman, Z. R. In "Developments in Block Copolymers"; Goodman, I., Ed.; Applied Science: London, 1982.
(26) Ramakrishnan, V. *J. Appl. Cryst.*, submitted.
(27) Stanley, H. E. "Introduction to Phase Transitions and Critical Phenomena"; Oxford University Press: Oxford, 1971.
(28) Whitmore, M. D.; Noolandi, J. *Macromolecules*, in press.
(29) Guinier, A.; Fournet, G. "Small-Angle Scattering of X-Rays"; Wiley: New York, 1955.
(30) Flory, P. J. "Principles of Polymer Chemistry"; Cornell University Press: Ithaca, NY, 1953.
(31) Herkt-Maetzky, C.; Shelton, J. *Phys. Rev. Lett.* **1983**, *51*, 896.
(32) Hadziioannou, G.; Stein, R.; Higgins, J. *Polym. Prepr. (Am. Chem. Soc., Div. Polym. Chem.)* **1983**, *24*, 213.
(33) Maconnachie, A.; Kambour, R. P.; White, D. M.; Rostami, S.; Walsh, D. J. *Macromolecules* **1984**, *17*, 2645.
(34) Sanchez, I. In "Polymer Blends"; Paul, D. R.; Newman, S., Eds.; Academic Press: New York, 1978; Vol. 1.
(35) Flory, P. J. *Discuss. Faraday Soc.* **1970**, *49*, 7.
(36) Bates, F. S.; Wignall, G. D.; Koehler, W. C. *Phys. Rev. Lett.*, in press.
(37) Rainville, E. D. "Special Functions"; Chelsea: New York, 1960.

Theory of Phase Equilibria in Block Copolymer–Homopolymer Blends

Mark Douglas Whitmore† and Jaan Noolandi*

Xerox Research Centre of Canada, 2660 Speakman Drive, Mississauga, Ontario, Canada L5K 2L1. *Received January 15, 1985*

ABSTRACT: The free energy of an inhomogeneous diblock copolymer–homopolymer blend is evaluated by using the functional integral formalism for multicomponent systems developed earlier. The advantage of this approach is that all important physical effects, such as polymer chain stretching, conformational entropy changes near an interface, enthalpic terms, etc., as well as the connectedness of the blocks of the copolymer, are automatically taken into account. In order to simplify the theory we calculate the inhomogeneous contribution to the free energy, as well as the polymer distribution functions, in a perturbation scheme (Landau–Ginzburg expansion), assuming that the density fluctuations of the components are small in comparison with their average values. This approach is valid near the spinodal for microphase separation and is less reliable as the inhomogeneous free-energy term grows in magnitude. For simplicity the ordered phase is assumed to have a lamellar structure, so that the third-order term in the expansion of the free energy vanishes. The temperature–composition phase diagrams for styrene–butadiene copolymer mixed with either polystyrene or polybutadiene homopolymer are calculated as an example for a series of chain lengths. The curvature of the phase boundaries near eutectic or critical points is discussed in detail. The assumption of a lamellar structure restricts the direct transition between the mesophase and the homogeneous phase to second order, resulting in the coalescence of some binodal lines in the phase diagrams. The maximum solubility of the homopolymer in the ordered phase is found to be large (up to 30% w/w) but to decrease rapidly as the homopolymer molecular weight is increased. The condition for homopolymer-induced mesophase formation is found to be $Z_H/Z_C \gtrsim {}^1/_4$ for a symmetric copolymer and a selective homopolymer with degrees of polymerization Z_C and Z_H, respectively. A computer program for evaluating the phase diagrams is available as supplementary material.

1. Introduction

Recent experimental work on diblock copolymer–homopolymer blends using small-angle X-ray and light-scattering techniques has given a great deal of information about their microstructure.[1,2] The equilibrium temperature–composition phase diagram shows a number of transitions between ordered and homogeneous phases, as well as different morphologies for the microdomains. When coupled with the results of other studies on block copolymers and their blends,[3-8] a picture of great diversity in the mechanical and structural properties of these "polymeric alloys" begins to emerge.

The purpose of this paper is to provide a theoretical basis for future realistic calculations of the equilibrium phase diagrams of block copolymer–homopolymer blends. In earlier work, we have formulated a general theory of multicomponent polymeric systems based on the functional integral formalism developed by Helfand for homopolymer interfaces and pure block copolymers.[9-11] This theory involves the solution of modified mean field diffusion equations for the polymer distribution functions. The connectedness of the blocks of the copolymer is included explicitly in the formalism, along with constraints that restrict density fluctuations and conserve the number of molecules. The derivation of the general free energy for the inhomogeneous system includes all important physical effects such as changes in the conformational entropy of the polymers in an interphase region, stretching of polymer chains throughout the microdomains, various configurational entropy terms corresponding to localization of homopolymers and block copolymers as well as block copolymer joints, and interaction terms between different chemical species. The expressions for the mean fields that occur in the diffusion equations for the distribution functions involve integrals of the polymer distribution functions, and in general these equations have to be solved numerically in a self-consistent scheme. This has been done for the case of homopolymer interfaces,[9] pure block copolymers,[10,11] block copolymers with a nonselective solvent,[12] and block copolymers at a demixed homopolymer interface.[13] In many cases the numerical work has served as a valuable guide to a deeper understanding of the

†Permanent address: Department of Physics, Memorial University of Newfoundland, St. John's, NF, Canada A1B 3X7.

0024-9297/85/2218-2486$01.50/0